# Modeling and Control of Multiple Aerial-Ground Manipulator System (MAGMaS) with Load Flexibility

Hyunsoo Yang, Nicolas Staub, Antonio Franchi, Dongjun Lee

Preprint, final version at http://ieeexplore.ieee.org/ 2018 IEEE/RSJ Int. Conf. on Intelligent Robots and Systems

# Modeling and Control of Multiple Aerial-Ground Manipulator System (MAGMaS) with Load Flexibility

Hyunsoo Yang[1], Nicolas Staub[2], Antonio Franchi[2] and Dongjun Lee[1]

***Abstract*— The MAGMaS (Multiple Aerial-Ground Manipulator System) was proposed in [1] as a heterogeneous system composed of multiple ground (mobile) manipulators and aerial robots to collaboratively manipulate a long/large-sized object and demonstrated therein for rigid load manipulation. Here, we extend this result of [1] to the case of load manipulation with flexibility, which is crucial for long/slender object manipulation, yet, not considered in [1]. We first provide a rigorous modeling of the load flexibility and its effects on the MAGMaS dynamics. We then propose a novel collaborative control framework for flexible load-tip pose tracking, where the ground manipulator provides slower nominal pose tracking with overall load weight holding, whereas the aerial robot allows for faster vibration suppression with some load weight sharing. We also discuss the issue of controllability stemming from that the aerial robot provides less number of actuation than the modes of the load flexibility; and elucidate some peculiar conditions for this vibration suppression controllability. Simulations are also performed to demonstrate the effectiveness of the proposed theory.**

## I. Introduction

Free flying control problem of small-size multi-rotor aerial robots is now well established with many strong theoretical results (e.g., [2]–[5]) and commercial systems (e.g., [6], [7]). This multi-rotor aerial robot has been particularly successful for the aerial photography and visual inspection applications by extending humans' eyes to the sky. The next step, naturally along this line of reasoning, would then be to extend humans' hands to the sky, namely, the problem of aerial operation and manipulation (e.g., [**?**], [8]–[11]), which can be useful for such applications as infrastructure maintenance [12], remote construction [13], object transport and assembly [14]–[16], etc.

Now, let us consider the problem of large-size structure construction. For this, the (virtually) unlimited workspace of the aerial robots would be useful. However, at the same time, such construction usually requires manipulation of large-sized objects (e.g., steel bar, wood beams, etc.) typically too heavy to be carried by many usual aerial robots alone due to the inherent rotor-battery limitation. On the other hand, ground (mobile or fixed) manipulators are typically of high payload, yet, their workspace (or working height) limited. To address this challenge, the MAGMaS (Multiple Aerial-Ground Manipulator System) was proposed in [1] as a heterogeneous system composed of multiple ground (mobile) manipulators (with high payload, yet, limited workspace) and aerial robots (with large workspace, yet, limited payload) to collaboratively manipulate a large-size heavy object by leveraging their complementary capabilities, see Fig. 1. The MAGMaS, of course, can be useful for other applications as well, e.g., warehouse automation, manipulation of large/heavy repair/inspection tool, etc.

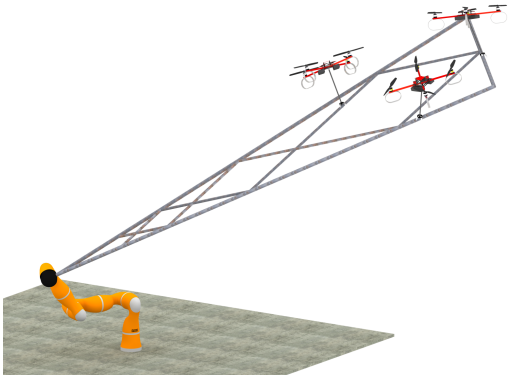

Fig. 1: MAGMaS composed of one ground manipulator and three aerial robots with a co-manipulated large object.

The focus of our previous work [1], however, was, on top of proposing this new class of MAGMaS and its implementation, to propose a control framework for the large/slender *rigid* object manipulation by employing the complementary capabilities and redundancy of both ground-aerial robots. In this paper, we extend this result of [1] to the case of load manipulation with *flexibility*, which is crucial for long/slender object manipulation and was not yet addressed. For this, we first provide a rigorous modeling of the MAGMaS with the (slender) load flexibility incorporated into that using Euler-Bernoulli beam theory. We then propose a novel collaborative control framework for the flexible load-tip pose tracking, where the ground manipulator provides slower nominal pose tracking with overall load weight holding, whereas the aerial robot[1] faster vibration suppression with some load weight sharing. We also elucidate the issue of controllability stemming from the fact that the aerial robot provides less degree of actuation than that the number modes of the load flexibility; and delineate some peculiar conditions for this vibration suppression controllability with their physical meaning manifested. Simulations are also performed to demonstrate the effectiveness of the proposed theory.

Research supported in part by by the Basic Science Research Program (2015R1A2A1A15055616) and the Engineering Research Center Program (2016R1A5A1938472) of the National Research Foundation, MSIP, Korea; the Industrial Strategic Technology Development Program (10060070) of MOTIE, Korea; and the European Union Horizon 2020 research and innovation program under grant agreement No. 644271 AEROARMS.

[1] Department of Mechanical & Aerospace Engineering and IAMD, Seoul National University, Seoul, Republic of Korea. yangssoo@snu.ac.kr, djlee@snu.ac.kr, Corresponding author: Dongjun Lee.

[2] LAAS-CNRS, Université de Toulouse, CNRS, Toulouse, France, nicolas.staub@laas.fr, antonio.franchi@laas.fr

[1]It is also worthwhile to mention that this aerial robot, by providing collocated load-tip actuation, can allow us to circumvent the well-known issue of nonminimum-phase dynamics for load-tip pose tracking control if only ground robot is employed [17], [18], [21].

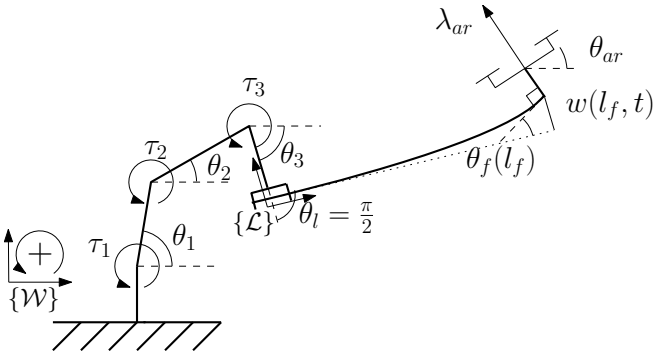


Fig. 2: Sketch of the configuration of the MAGMaS.

The rest of the paper is organized as follow, Sec. II describes in depth the system at hand. In Sec. III, the dynamical model of the system, including the vibrations in the load is derived and Sec. IV makes use of it to construct the control scheme. Sec. V presents realistic simulation results which validate our approach, finally Sec. VI highlights our conclusion and path for future works.

## II. System Description

In this section, we recall and detail the composition of the Multiple Aerial Ground Manipulators System (MAGMaS) introduced in [1]. We then provide the dynamical modeling developed in Sec. III. A MAGMaS consists of a $n$-degrees of freedom (DoFs) ground manipulator, some load/object to manipulate and one or several aerial robot (e.g., quadrotor) connected to the load, see. Fig 1. This system is proposed to outperform the other approaches on aerial manipulation by taking advantage of its heterogeneity: 1) higher payload and unlimited operation time of the robotic manipulator; 2) dealing with large objects or workspace with a group of aerial robots [1].

We assume a manipulated object as a long bar with skewed rectangular shape cross-section so that the vibration only along one direction is substantial, while that along the other one is negligible. We also confine ourselves to the case of planar manipulation in this paper. The ground manipulator considered is then a planar $n$-dof manipulator. We also limit our study to a MAGMaS composed of a single aerial robot, which grasps (or is attached to) the bar-end. Even with this reduction, as can be seen below, the obtained key technical results and frameworks would be extendable to more general cases as well. The aerial robot is connected to the bar by the mean of small arm mounted on a passive rotational joint, whose center of rotation coincides with aerial robot center-of-mass (CoM), see Fig. 2. This is a requirement to limit the torque exerted by the aerial robot on the load as the actuation limits on the torque of such platform are typically quite low. This also implies that the load and the aerial robot exchange only force, not moment.

The notations used throughout the paper are depicted in Fig. 2. On the ground, $n$-DoF robot arm is mounted whose joint configuration is defined as $\theta \in \Re^n$. The position of each joint and the center-of-mass of each links w.r.t. the inertial frame $\mathcal{W}$ are defined as $p_i^{\mathcal{W}} \in \Re^2$ and $p_{c,i}^{\mathcal{W}} \in \Re^2$ respectively. Similarly, the end-effector position of the robot arm is defined as $p_e^{\mathcal{W}} \in \Re^2$. For brevity, we will omit the superscript $\mathcal{W}$ when the position is represented in the inertial frame. Define the position and the orientation of the aerial robot attached on the load-tip w.r.t. $\mathcal{W}$ as $p_{ar} \in \Re^2$ and $\bar{\theta}_{ar} \in \Re$. Throughout this paper, for any angle, e.g. $\theta$, the notation $\bar{\theta}$ represents the absolute angle, e.g., $\bar{\theta}_i = \sum_{j=1}^{i} \theta_j$, while $\theta$ represents relative angle.

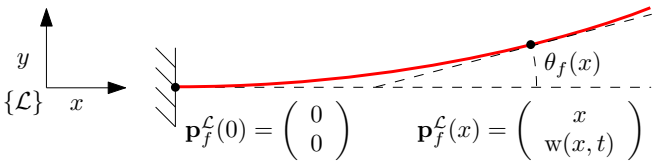


Fig. 3: Euler-Bernoulli beam deflection model.

The flexible load is rigidly attached to end-effector of the robot arm. The relative angle between the end-effector and the flexible load is given as $\theta_l$. As shown in Fig. 3, the position and orientation of the flexible load along the $x$-axis w.r.t. the flexible load frame $\mathcal{L}$ at time $t$ can be written as

$$p_f^{\mathcal{L}}(x,t) = \begin{bmatrix} x \\ w(x,t) \end{bmatrix}, \quad \theta_f(x,t) = \frac{\partial w(x,t)}{\partial x}$$

where $w(x,t)$ is the deflection along $y$-direction at $x$ in the load frame $\mathcal{L}$. We omit $x$ at the load-tip position $x = l_f$ for brevity, i.e., $p_f^{\mathcal{L}}(l_f) = p_f^{\mathcal{L}}$ and $\theta_f(l_f) = \theta_f$. Recall that the aerial robot is connected to the flexible load via a passive rotational joint, which allows free relative rotation of the aerial robot as stated above, $\bar{\theta}_{ar}$ can be independently controlled by the aerial robot. The length of the arm between the load-tip and the aerial robot CoM is $d_{conn}$ which is assumed zero in the rest of the paper, thus neglecting torque generated on the load by the aerial robot thrust via the rigid connecting arm.

## III. System Modeling

The dynamic model of the MAGMaS based on the Euler-Bernoulli beam theory and Euler-Lagrange equation is derived in this section. We first briefly introduce the Euler-Bernoulli equation which is not a main contribution of this paper, and then derive the dynamic equation of the whole MAGMaS.

### A. Flexibility Modeling of the Load

Here, we suppose to include only transverse vibration, i.e., torsional effects are neglected, with restriction of motion of the MAGMaS to planar space. This assumption can be enforced by a proper structural design of the load (e.g., long slender beam) [19]. To model vibration of the flexible load, here, we adopt Euler-Bernoulli beams theory [19], whose governing equation is given as follows

$$\rho A(x) \frac{\partial^2 w(x,t)}{\partial t^2} + \frac{\partial^2}{\partial t^2} EI(x) \frac{\partial^2 w(x,t)}{\partial t^2} = 0 \qquad (1)$$

where $E, I, \rho, A$ are Young's modulus, the second moment of area, the density and the intersection area of the flexible load respectively. These material properties are invariant for the homogeneous load with uniform cross section, thus, in this paper, we assume the constant parameters along the flexible load to simplify the beam model and to meet the practical objects (e.g., long rectangular wooden rod).

Using the separation of variables, a solution of given partial differential equation (1) can be written s.t.,

$$w(x,t) = \sum_{i=1}^{m} \phi_i(x)\delta_i(t) =: \Phi(x)\delta(t) \tag{2}$$

where $w(x,t) \in \Re$ is the load deflection along the $y$-direction location at $x$ w.r.t the load frame $\mathcal{L}$ and time $t$ , $m$ is the number of assumed vibration modes, $\phi_i(x)$ is the time invariant mode shape function, $\delta_i(t)$ describes the time varying part of the deflection associated with given mode shape $\phi_i(x)$, $\Phi := [\phi_1, \cdots, \phi_m] \in \Re^m$ is the combined row vector of mode shapes and $\delta := [\delta_1; \cdots; \delta_m] \in \Re^m$ is the combined column vector of $\delta_i$. In practice, high frequency modes are suppressed quickly due to their damping. Therefore, we only consider a finite dimension $m$ of the vibration modes.

The explicit solution form of $\phi_i(x)$ can be written as follows

$$\begin{aligned}\phi_i(x) = C_{1,i}\cosh\beta_i x + C_{2,i}\cos\beta_i x \\ + C_{3,i}\sinh\beta_i x + C_{4,i}\sin\beta_i x\end{aligned}$$

where $C_i$ are the coefficients, $\beta_i^4 = w_{n,i}^2\rho A/EI$, and $w_{n,i}$ is the natural frequency of $i$-th vibration mode. All these parameters are determined by the boundary condition of Euler-Bernoulli equation (1). To determine these coefficients, we adopt two boundary conditions: 1) the clamped boundary conditions at $x = 0$, (i.e., at the end-effector position); 2) the mass boundary conditions for moment and shear force at the load-tip $l_f$ induced by aerial robot. These are expressed as following four conditions [20]:

$$w(x=0,t) = 0, \quad \theta_b(x=0,t) \approx \frac{dw}{dx} = 0 \tag{3}$$

$$M(x=l_f) = 0 \tag{4}$$

$$V(x=l_f) = -m_{ar}\ddot{w}_b(l_f,t) + m_{ar}ge_2 \tag{5}$$

where $\theta_b$ is deflection angle, $M(l_f) = EI\frac{\partial w^2}{\partial x^2}$ is the moment, $V(l_f) = -EI\frac{\partial w^3}{\partial x^3}$ is the shear force at the load-tip. Using these four equations derived from the boundary conditions, five coefficients $C_{1,i}, C_{2,i}, C_{3,i}, C_{4,i}, \beta_i$ can only be determined up to scale [20]. The scale of the coefficients can be determined by normalization based on the following relation

$$\rho A\int_0^{l_f}\phi_i(x)^2dx + m_{ar}\phi_i(l_b)^2 = \frac{EI}{w_{n,i}^2}\int_0^{l_f}\phi_i''(x)^2dx \tag{6}$$

This relation is derived from (1), (3)-(5). By assuming the left hand side of (6) to be unity, the mode shape $\phi_i$ is normalized, then we can determine scale of coefficients $C_{i,j}$.

Here, the mode shape is the eigenfunction describing the deflection based on Euler-Bernoulli equation (1). Therefore, orthogonality is enforced to each mode shapes for $i \neq j$, see [20], s.t.:

$$\int_0^{l_f}\phi_i''(x)\phi_j''(x)dx = 0 \tag{7}$$

$$\int_0^{l_f}\phi_i(x)\phi_j(x)dx + m_{ar}\phi_i(l_f)\phi_j(l_f) = 0 \tag{8}$$

Based on these orthogonality, the inertia and the stiffness are expressed as diagonal matrix in the Sec. III-D.

As a result, we define the system configuration as $q = [\theta^T, \delta^T]^T \in \Re^{n+m}$ where $\delta \in \Re^m$ is the time-dependant deflection variable for the flexible load defined in (2).

### *B. Kinetic Energy of the MAGMaS*

To derive Euler-Lagrange equation of the MAGMaS, first, the kinetic energy of the MAGMaS is obtained s.t.,

$$T = T_{arm} + T_{bar} + T_{ar}$$

where $T_{arm}, T_{bar}, T_{ar}$ are the kinetic energies of the manipulator, the flexible load and the aerial robot respectively. Explicit expression of each kinetic energies are given as following:

$$\begin{aligned}T_{arm} &= \sum_{i=1}^{3}\frac{1}{2}m_i\dot{p}_{c,i}^T\dot{p}_{c,i} + \frac{1}{2}I_{c,i}w_i^2 \\ T_{bar} &= \frac{\rho A}{2}\int_0^{l_b}\dot{p}_f(x)^T\dot{p}_f(x)dx \\ T_{ar} &= \frac{1}{2}m_{ar}p_f^Tp_f + \frac{1}{2}I_{ar}w_{ar}^2\end{aligned}$$

where $p_f(x) \in \Re^2$ is the position of the flexible bar along the $x$-axis of the load frame w.r.t. the inertial frame $\mathcal{W}$ with its expression and the time derivative are given as following

$$\begin{aligned}p_f(x) &= p_e + R_{\mathcal{L}}^{\mathcal{W}}\begin{bmatrix}x \\ w(x,t)\end{bmatrix} \\ \dot{p}_f(x) &= \dot{p}_e + R_{\mathcal{L}}^{\mathcal{W}}\left(S(\omega_f)\begin{bmatrix}x \\ w(x,t)\end{bmatrix} + \begin{bmatrix}0 \\ \dot{w}(x,t)\end{bmatrix}\right) \\ &= \underbrace{\left(\begin{bmatrix}J_e & 0\end{bmatrix} + \begin{bmatrix}R_{\mathcal{L}}^{\mathcal{W}}\begin{bmatrix}-w(x,t) \\ x\end{bmatrix} 1_m^T & e_2\Phi(x)\end{bmatrix}\right)}_{=:J_f(x)\in\Re^{2\times(n+m)}}\begin{bmatrix}\dot{\theta} \\ \dot{\delta}\end{bmatrix}\end{aligned} \tag{9}$$

where $J_e \in \Re^{2\times n}$ is the robot arm Jacobian for the end-effector, $w_f = \sum_{i=1}^{n}\dot{\theta}_i$ is the angular velocity of the flexible load frame $\mathcal{L}$ which is same as the angular velocity of the end-effector, $1_m = [1; \cdots; 1] \in \Re^m$ is one vector, $e_2 = [0; 1] \in \Re^2$ is the unit vector and $\Phi(x) = [\phi_1(x), \cdots, \phi_m(x)] \in \Re^m$ is the mode shape row vector at $x$. Here, recall that we deal with the planar motion, thus we only consider pitch motion for the aerial robot which is expressed as $\bar{\theta}_{ar} \in \Re$ and its time derivative $w_{ar} \in \Re$.

### *C. Potential Energy*

The potential energy of the MAGMaS is expressed as the summation of the gravitational potential energies and the elastic potential energy of the flexible load:

$$U = U_{arm} + U_{bar,el} + U_{bar,g} + U_{ar}$$

The gravitational potential energies are expressed as

$$U_{arm} = \sum_{i=1}^{n} m_i g e_2^T p_{c,i},\ U_{ar} = m_{ar}ge_2^Tp_f(l_f)$$

$$U_{bar,g} = \rho A g e_2^T\left(p_e + \int_0^{l_b} R_{\mathcal{L}}^{\mathcal{W}}p_f^{\mathcal{L}}(x)dx\right)$$

where $g \in \Re$ is the gravitational acceleration. Note that the position of the aerial robot is same as the load-tip position $p_{ar} = p_f(l_f)$ due to the assumption of $d_{conn} \approx 0$. The elastic energy of the flexible load can be written as

$$U_{bar,el} = \frac{EI}{2}\int_0^{l_b}\left(\frac{\partial^2 w}{\partial x^2}\right)^2 dx = \frac{EI}{2}\sum_{i=1}^{m}\sum_{j=1}^{m} d_{ij}\delta_i\delta_j$$

where $d_{ij} := \int_0^{l_b} \phi_i''\phi_j'' dx$ is satisfying the orthogonality in (7).

### D. Euler-Lagrange Dynamics

Using the kinetic $T$ and the potential energy $U$, the Lagrangian is defined as $L = T - U$. Then, we can derive following Euler-Lagrange dynamics of the MAGMaS:

$$\begin{bmatrix} M_\theta & M_{\theta\delta} \\ M_{\delta\theta} & M_\delta \end{bmatrix}\ddot{q} + \begin{bmatrix} C_\theta & C_{\theta\delta} \\ C_{\delta\theta} & 0 \end{bmatrix}\dot{q} + g(q) + \begin{bmatrix} 0 & 0 \\ 0 & K \end{bmatrix} q = B(q)\begin{bmatrix} \tau_m \\ \tau_{ar} \end{bmatrix} \quad (10)$$

where $M_\theta \in \Re^{n\times n}$, $M_\delta \in \Re^{m\times m}$, $M_{\theta\delta} = M_{\delta\theta}^T \in \Re^{m\times n}$ are the inertia matrix, $C_\theta \in \Re^{n\times n}$, $C_{\delta\theta} \in \Re^{m\times n}$, $C_{\theta\delta} \in \Re^{n\times m}$ are the Corilois matrix, $g(q) \in \Re^{n+m}$ is the gravity force vector, $B(q) \in \Re^{(n+m)\times(n+2)}$ is the input mapping matrix, $\tau_m \in \Re^n$ is the joint torque and $\tau_{ar} = \lambda_{ar} R_{ar} e_2 \in \Re^2$ is the aerial robot thrust input with the rotation matrix $R_{ar} \in SO(2)$, and the thrust magnitude $\lambda_{ar} \in \Re$ . The inertia matrix for flexibility $M_\delta$ and the stiffness matrix $K$ are constant diagonal matrix where the off-diagonal terms are eliminated by the orthogonality properties (7) and (8). Note that the aerial robot rotation is independent to above dynamics thanks to the passive rotational joint design of the connector, thus the aerial robot rotational dynamics is excluded in (10). We can consider the aerial robot as a rotating thrust generator similar with [8]. The input mapping matrix $B(q)$ have the following structure

$$B(q) = \begin{bmatrix} I_n & J_f^T \\ 0 & B_{\delta,ar} \end{bmatrix}$$

where $I_n \in \Re^{n\times n}$ is the identity matrix, $J_f$ is the Jacobian of the load-tip defined in (9), $B_{\delta,ar} \in \Re^{m\times 2}$ is the input matrix for the flexibility dynamics with the following expression

$$B_{\delta,ar} = \begin{bmatrix} -\phi_1(l_f)\sin\bar{\theta}_l & \phi_1(l_f)\cos\bar{\theta}_l \\ \vdots & \vdots \\ -\phi_m(l_f)\sin\bar{\theta}_l & \phi_m(l_f)\cos\bar{\theta}_l \end{bmatrix} \quad (11)$$

where $\bar{\theta}_l = \sum\theta_i + \theta_l$ is the absolute orientation of the flexible load at the end-effector. From the input mapping matrix $B(q)$, the manipulator control input $\tau_m$ cannot directly apply its torque to the flexible load dynamics while the aerial robot input $\tau_{ar}$ directly control the flexible load along $B_{\delta,ar}$. Note that the matrix $B_{\delta,ar}$ is a rank one matrix along $\Phi^T$ although it is $m$ by 2 matrix. Therefore, the $m$-DoFs flexible load dynamics is under-actuated with rank one input unless the number of the mode shape $m$ is one.

## IV. Control Design

For the MAGMaS, our control objective is the position/orientation trajectory tracking of the flexible load-tip (c.f., rigid object control in previous work [1]). For this control objective, if we only have the robot arm control input $\tau_m$, i.e., the dynamics (10) without aerial robot input $\tau_{ar}$, the zero dynamics is unstable [21]. On the other hand, the MAGMaS can overcome this fundamental issue by incorporating the aerial robot as a force generator to the flexible load dynamics as shown in (10) with $\tau_{ar}$.

However, as shown in the structure of $B_{\delta,ar}$ in (11), we only have rank one control input to stabilize $m$-dim flexible load vibration dynamics. To resolve this under-actuation problem, we divide this control objective into the following two sub-problems: 1) slow fully-actuated robot arm control; 2) under-actuated flexible load vibration suppression via the fast aerial robot control. First, for the fully actuated manipulator dynamics, by considering the flexible load at the equilibrium similar to a rigid body, we can design a desired trajectory for the robot arm end-effector $(p_e^d, \bar{\theta}_e^d)$ based on the inverse kinematics. Then, the robot arm is enforced to follow the computed desired trajectory. Next, for the under-actuated flexible load dynamics, since we cannot generate arbitrary control input due to less number of the actuation than the modes of the load flexibility, we perform the controllability analysis for the linearized dynamics by assuming perfect trajectory tracking of the robot arm which is established in first step. Then, we design the vibration suppression controller (i.e., for $\dot{\delta}_i \to 0$) for the aerial robot. When we compute the equilibrium of the flexible load in the first step, we also design the aerial robot thrust to compensate the deflection at the flexible load-tip $w(l_f) \to 0$ whose physical meaning is the gravity induced deflection compensation. In the second step, the controllability analysis validates that the proposed controller can stabilize vibration near the equilibrium deflection. Here, as the vibration dynamics is relatively faster than the end-effector trajectory, this linearization approach is feasible.

### A. Manipulator Control

For the end-effector trajectory tracking of the manipulator, we first transform the joint space dynamics (10) into the manipulator workspace dynamics using Jacobian mapping:

$$\dot{\xi} = J_\xi\dot{\theta}, \quad \ddot{\xi} = \dot{J}_\xi\dot{\theta} + J_\xi\ddot{\theta}$$

where $\xi := [p_e, \bar{\theta}_e] \in \Re^3$ is the end-effector position/orientation w.r.t. the inertial frame $\mathcal{W}$, $J_\xi \in \Re^{3\times n}$ is the manipulator Jacobian for the joint angle $\theta$ to $\xi$. Here, we assume the non-redundant manipulator (i.e., $n = 3$) to focus on the cooperative control with the aerial robot rather than deal with the manipulator's redundancy. Then, the MAGMaS dynamics in workspace coordinates can be written as follows

$$\begin{bmatrix} M_\xi & M_{\xi\delta} \\ M_{\delta\xi} & M_\delta \end{bmatrix}\begin{pmatrix}\ddot{\xi}\\ \ddot{\delta}\end{pmatrix} + \begin{bmatrix} C_\xi & C_{\xi\delta} \\ C_{\delta\xi} & 0 \end{bmatrix}\begin{pmatrix}\dot{\xi}\\ \dot{\delta}\end{pmatrix} + S^T g(q) + \begin{bmatrix} 0 & 0 \\ 0 & K \end{bmatrix}\begin{pmatrix}\xi\\ \delta\end{pmatrix} = S^T B(q)\begin{bmatrix}\tau_m \\ \tau_q\end{bmatrix}$$

where $S = \text{diag}(J_\xi^{-1}, I_m) \in \Re^{(n+m)\times(n+m)}$ is transformation matrix. Using this workspace dynamics, we can the design following control input

$$\tau_m = \bar{M}_\xi \ddot{\xi}_d + \bar{C}_\xi \dot{\xi} + D_e \dot{e} + K_e e - C_{\xi\delta}\dot{\delta} - M_{\xi\delta}\bar{K}\delta + \bar{g}_e - (J_\xi^{-T} J_f^T(q) - M_{\xi\delta}\bar{B}_{\delta,ar})\tau_{ar} \quad (12)$$

where $e = \xi - \xi^d$ is the end-effector position/orientation error, $\bar{M}_\xi = M_\xi - M_{\xi\delta}M_\delta^{-1}M_{\delta\xi}$, $\bar{C}_\xi = C_\xi - M_{\xi\delta}M_\delta^{-1}C_{\delta\xi}$, $\bar{g}_\xi = J_e^{-1}g_\theta - M_{\xi\delta}M_\delta^{-1}g_\delta$, $\bar{K} = M_\delta^{-1}K$ and $D_e, K_e \in \Re^{3\times3}$ are positive definite control gain matrices. Here, the desired end-effector trajectory can be computed from the desired load-tip trajectory by assuming the deflection is zero (i.e., $w(l_f) = 0$) which is enforced by the aerial robot control. Note that this inverse kinematics is similar to the one of alone ground manipulator. Then, the closed-loop dynamics for the manipulator workspace is given as follows

$$\bar{M}_\xi \ddot{e} + D_e \dot{e} + K_e e = 0$$

Given that the closed loop dynamics converges to $e \to 0$ with positive definite $\bar{M}_\xi, D_e, K_e$. Note that the manipulator dynamics corresponds to the one of a standard fully-actuated standard manipulator dynamics, thus the controller can be easily extended to redundant manipulator [22] for $n > 3$ or other controllers (e.g., robust control, adaptive control, etc.).

### B. Flexible Load Dynamics Analysis

From previous section IV-A, the proposed robot arm control guarantees $\xi \to \xi^d$. Therefore, the vibration dynamics can then be rewritten as follows with $\xi = \xi^d$

$$\begin{bmatrix}\ddot{\delta}\\ \dot{\delta}\end{bmatrix} = \begin{bmatrix}0_m & -M_\delta^{-1}K\\ I_m & 0_m\end{bmatrix}\begin{bmatrix}\dot{\delta}\\ \delta\end{bmatrix} + \begin{bmatrix}M_\delta^{-1}B_{\delta,ar}\\ 0\end{bmatrix}\tau_{ar} - \begin{bmatrix}M_\delta^{-1}E\\ 0_m\end{bmatrix} =: \begin{bmatrix}0_m & -\bar{K}\\ I_m & 0_m\end{bmatrix}\begin{bmatrix}\dot{\delta}\\ \delta\end{bmatrix} + \begin{bmatrix}\bar{B}_{\delta,ar}\\ 0\end{bmatrix}\tau_{ar} - \begin{bmatrix}\bar{E}\\ 0\end{bmatrix} \quad (13)$$

where $E$ is defined as

$$E := M_{\delta\xi}\ddot{\xi}^d + C_{\delta\xi}\dot{\xi}^d + g_\delta(\bar{\theta}_e^d)$$

We can further simplify the control input expression using the definition of $B_{\delta,ar}$ in (11) and $\tau_{ar}$ as following

$$\bar{B}_{\delta,ar}\tau_{ar} = M_\delta^{-1}B_{\delta,ar}R(\bar{\theta}_{ar})e_2\lambda_{ar} = M_\delta^{-1}\underbrace{\Phi^T\cos(\bar{\theta}_{ar} - \bar{\theta}_l)}_{=:b_{\delta,ar}\in\Re^m}\lambda_{ar} = \bar{b}_{\delta,ar}\lambda_{ar} \quad (14)$$

where $R(\bar{\theta}_{ar}) \in SO(2)$ denotes a rotation matrix and $\theta_{ar}^{\mathcal{L}} = \bar{\theta}_{ar} - \bar{\theta}_l$ is the relative orientation of aerial robot w.r.t. the flexible load frame $\mathcal{L}$. Recall that $\bar{\theta}_{ar}$ is independently controlled, thus if we regulate $\dot{\theta}_{ar}^{\mathcal{L}} = 0$, then the input mapping vector $\bar{b}_{\delta,ar}$ can be considered as a constant.

*1) Linearization:* Due to the under-actuation with the rank one aerial robot input $\bar{b}_{\delta,ar}\lambda_{ar}$ for the $m$-DoFs flexible load dynamics (13), we cannot completely cancel out the coupling between the manipulator and the flexible load $\bar{E}$. Therefore, we design a flexible load vibration/deflection suppression controller with controllability analysis. To analyze controllability, we need to linearize the dynamics (13) at the equilibrium deflection $\delta_e \in \Re^m$ along the end-effector trajectory $\xi^d$. Here, we can assume relatively slower ground manipulator end-effector motion than vibration (i.e., $\dot{\xi} \ll \dot{\delta}$) because the robot arm can generate desired velocity for the load-tip with slow manipulator end-effector motion as length of the load increases.

We aim to behave the flexible load similar to the rigid body, thus the control objective of the aerial robot includes both the vibration suppression $\dot{\delta} = 0$ and the deflection compensation $w(l_f) = 0$. Note that zero deflection at the tip $w(l_f) = 0$ does not imply zero deflection for all location along the load (i.e., not $\delta_i(x) = 0$ for all $x$). Therefore, $w(l_f) = 0$ is the equilibrium point of the linearized flexible load dynamics which is also the assumption of the inverse kinematics of $(p_e^d, \bar{\theta}_e^d)$ in Sec. IV-A.

First of all, we design a feedforward control input to compensate the gravity force at the equilibrium deflection $\delta_e$ to satisfy $w(l_f) = 0$. The equilibrium deflection satisfies following equality

$$K\delta_e + g_\delta(\theta) = b_{\delta,ar}\lambda_{ar}$$

We then get the following expression for the deflection $w(l_f)$ by premultiplying $\Phi K^{-1}$

$$\Phi\delta_e = \Phi K^{-1}(b_{\delta,qr}\lambda_{ar} - g_\delta(\theta))$$

Then, the feedforward control input for the gravity induced deflection compensation can be proposed as

$$\lambda_{ar} = (\Phi K^{-1}b_{\delta,ar})^{-1}\Phi K^{-1}g_\delta \quad (15)$$

Note that stiffness matrix $K$ is a diagonal invertible matrix, thus $\Phi K^{-1}b_{\delta,ar} = \sum \phi_i^2(l_f)/K_{ii}\cos(\theta_{ar}^{\mathcal{L}})$ is also invertible unless $\cos(\theta_{ar}^{\mathcal{L}}) = 0$. Then, the equilibrium deflection vector $\delta_e$ can be written as following

$$\delta_e = (-I + K^{-1}b_{\delta,ar}(\Phi K^{-1}b_{\delta,ar})^{-1}\Phi)K^{-1}g_\delta(\theta)$$

Note that the equilibrium deflection $\delta_e$ enforced by $\lambda_{ar}$ satisfies zero deflection at the load-tip, i.e.,$w(l_f) = \Phi\delta_e = 0$.

Finally, we can linearize the dynamics (13) at the equilibrium deflection $\delta_e$

$$\begin{bmatrix}\ddot{\tilde{\delta}}\\ \dot{\tilde{\delta}}\end{bmatrix} = \underbrace{\begin{bmatrix}0_m & -\bar{K}\\ I_m & 0_m\end{bmatrix}}_{=:F}\begin{bmatrix}\dot{\tilde{\delta}}\\ \tilde{\delta}\end{bmatrix} + \underbrace{\begin{bmatrix}\bar{b}_{\delta,ar}\\ 0\end{bmatrix}}_{=:G}\bar{\lambda}_{ar} \quad (16)$$

where $\tilde{\delta} = \delta - \delta_e$ and $\bar{\lambda}_{ar} = \lambda_{ar} - (\Phi K^{-1}b_{\delta,ar})^{-1}\Phi K^{-1}g_\delta$.

*2) Controllability:* The linearized flexible load dynamics (16) is represented by $2m$ configurations $(\dot{\tilde{\delta}}, \tilde{\delta})$ with the rank one aerial robot input $G\lambda_{ar}$. Therefore, we need to verify whether the input $G\lambda_{ar}$ can suppress the vibration/deflection to the equilibrium $(\dot{\tilde{\delta}}, \tilde{\delta}) \to (0, 0)$ in the linearized system before designing a controller. For this, we utilize the controllability matrix $\mathcal{C}$ of the linearized deflection dynamics (16) defined as following

$$\mathcal{C} := [G\ FG\ \cdots\ FG^{m-1}] \in \Re^{2m\times2m}.$$

Combining with (16), the controllability matrix $\mathcal{C}$ can be rewritten as

$$\mathcal{C} = \begin{bmatrix}\bar{b}_{\delta,ar} & 0 & \cdots & (-\bar{K})^{m-1}\bar{b}_{\delta,ar} & 0\\ 0 & \bar{b}_{\delta,ar} & \cdots & 0 & (-\bar{K}^{m-1})\bar{b}_{\delta,ar}\end{bmatrix}$$

The given linearized flexible load dynamics (16) is controllable, if the controllability matrix satisfies $\text{rank}(\mathcal{C}) = 2m$.

To figure out the condition for the controllability, we need to check the condition for $\det(\mathcal{C}) \neq 0$. Here, we can simplify the evaluation of $\det(\mathcal{C})$ by utilizing the column permutation of the matrix $\mathcal{C}$ which only have impact on the sign of the determinant. Using the column permutation, we can collect all the odd columns and even columns, then the controllability matrix $\mathcal{C}$ can be expressed as block diagonal matrix of following submatrix $\mathcal{C}_s$:

$$\mathcal{C}_s = \begin{bmatrix} \bar{b}_{\delta,ar} & \bar{K}\bar{b}_{\delta,ar} & \cdots & \bar{K}^{m-1}\bar{b}_{\delta,ar} \end{bmatrix}$$

From the property of block diagonal matrix, $|\det(\mathcal{C})| = |\det(\mathcal{C}_s)|^2$, thus we only need to analyse $\det(\mathcal{C}_s)$. The determinant of $\mathcal{C}_s$ is described in the following Lemma.

**Lemma 1** *Consider the submatrix of the controllability matrix $\mathcal{C}_s$ of the linearized system* (16)*. Then the determinant of the matrix $\mathcal{C}_s$ satisfies following equation*

$$det(\mathcal{C}_s) = \prod_{i=1}^{m} \bar{b}_i \cdot \prod_{j=1}^{m} \left( \frac{EId_{jj}}{M_{\delta,jj}} - \frac{EId_{(j+1)(j+1)}}{M_{\delta(j+1)(j+1)}} \right) \quad (17)$$

*where $\bar{b}_i$ is $i$-th component of $\bar{b}_{\delta,ar}$, $M_{\delta,ii}$ is $(i,i)$ component of the inertia matrix $M_\delta$ and $d_{ii} = \int \phi_i''(x)^2 dx$. If $j = m$, then $j+1$ is considered as* 1.

**Proof:** If $m = 2$, we can compute $\det(\mathcal{C}_s)$ as following

$$\det(\mathcal{C}_s) = \begin{vmatrix} \bar{b}_1 & \frac{EId_{11}}{M_{\delta,11}}\bar{b}_1 \\ \bar{b}_2 & \frac{EId_{22}}{M_{\delta,22}}\bar{b}_2 \end{vmatrix} = \bar{b}_1\bar{b}_2\left(\frac{EId_{22}}{M_{\delta,22}} - \frac{EId_{11}}{M_{\delta,11}}\right)$$

Next, we assume (17) is satisfied for $m = n-1$. If this relations is also available for $m = n$, then the equation (17) is satisfied for any positive integer $m$. For $m = n$ the determinant is given as following

$$\begin{aligned} \det(\mathcal{C}_s) &= \begin{vmatrix} \bar{b}_{\delta,ar} & \bar{K}\bar{b}_{\delta,ar} & \cdots \bar{K}^{n-1}\bar{b}_{\delta,ar} \end{vmatrix} \\ &= \det\left(\text{diag}(\bar{b}_1, \cdots, \bar{b}_n) \cdot \begin{bmatrix} 1_n & \bar{K}1_n \cdots \bar{K}^{n-1}1_n \end{bmatrix}\right) \\ &= \prod_{i=1}^{n} \bar{b}_i \cdot \det \underbrace{\left(\begin{bmatrix} 1_n & \bar{K}1_n \cdots \bar{K}^{n-1}1_n \end{bmatrix}\right)}_{=:\mathcal{K}_n} \end{aligned}$$

where $1_n = [1, \cdots, 1]^T \in \Re^n$ is $n$-dim one vector. First term of right hand side is same with (17), thus we need to verify second term. According to Laplace's formula, determinant of matrix is expressed as summation of determinant of submatrices

$$\begin{aligned} \det(\mathcal{K}_n) &= \sum_{j=1}^{n} (-1)^{(j+1)} \det(\mathcal{K}_{n,(1,j)}) \\ &= \sum_{j=1}^{n} (-1)^{(j+1)} \begin{vmatrix} \bar{K}_{(j,j)}1_{n-1} & \cdots & \bar{K}_{(j,j)}^{n-1}1_{n-1} \end{vmatrix} \\ &= \sum_{j=1}^{n} (-1)^{(j+1)} \det(\bar{K}_{(j,j)}) \det(\mathcal{K}_{n,(n,j)}) \\ &= \sum_{j=1}^{n} (-1)^{(j+1)} \prod_{\substack{i=1 \\ i\neq j}}^{n} w_{n,i} \cdot \prod_{\substack{i=1 \\ i\neq j}}^{n} (w_{n,i} - w_{n,i+1}) \end{aligned} \quad (18)$$

where $\mathcal{K}_{n,(i,j)}, \bar{K}_{(i,j)} \in \Re^{(n-1)\times(n-1)}$ are matrices whose $i$-th column and $j$-th row are eliminated from the original matrices $\mathcal{K}_n$, $\bar{K}$ and $w_{n,i} := EId_{ii}/M_{\delta,ii}$ is the natural frequency of $i$-th mode. For the last equation, every $w_{n,i}$ have $(n-1)$-order. If we consider this equation as a function of $w_{n,i}$ (i.e., $f(w_{n,i}) = 0$), then $(n-1)$ order polynomial function have $(n-1)$ solutions. It is straightforward to show $w_{n,i} = w_{n,j}\ \forall j \in \{1, \cdots, i-1, i+1, \cdots, n\}$ are the solutions of this polynomial equation using (18) by substituting it to solution. As a result, equation (17) is satisfied for $m = n$ and, thus, satisfied for any positive integer $m$. ■

From Lemma 1, the three conditions to ensure controllability of the linearized system can be extracted in the following theorem:

**Theorem 1** *Consider the linearized flexible load dynamics* (16) *and controllability matrix $\mathcal{C}$. Then, if the following three conditions are met, the linearized flexible load dynamics is controllable:*

1) ***Design condition*** $\phi_i(l_f) \neq 0, \forall i = 1, \cdots, m$*;*
2) ***Control condition*** $\cos(\theta_{ar}^{\mathcal{L}}) \neq 0$*, i.e.,* $\theta_{ar}^{\mathcal{L}} \neq \frac{\pi}{2} + k\pi, k \in \mathcal{Z}$*; and*
3) ***Physical condition*** $\frac{EId_{ii}}{M_{\delta,ii}} \neq \frac{EId_{jj}}{M_{\delta,jj}}$ *(or* $w_{n,i} \neq w_{n,j}$*).*

**Proof:** According to Lemma 1, $\det(\mathcal{C}_s)$ is represented as product of $\bar{b}_i$ and $\frac{EId_{ii}}{M_{\delta,ii}} - \frac{EId_{jj}}{M_{\delta,jj}}$. The conditions for $\det(\mathcal{C}_s) = 0$ are induced by $\bar{b}_i = 0$ or $w_{n,i} = \frac{EId_{ii}}{M_{\delta,ii}} = \frac{EId_{jj}}{M_{\delta,jj}} = w_{n,j}$. From the expression of $\bar{b}_i$ in (14) and given that $M_\delta > 0$, we can conclude the condition translates to $\phi_i(l_f) = 0$ and/or $\cos(\theta_{ar}^{\mathcal{L}}) = 0$ which are the design and the control condition. The later one directly correspond to the physical condition. ■

To satisfy what we called the *design condition*, the mode shape at the aerial robot attachment position should not be zero, i.e., $\phi_i(l_f) \neq 0$. This controllability condition enforces a design criterion; the aerial robot should not be attached some mode node position along the beam, i.e., $\phi_i(x) = 0, \forall i = 1, \cdots, m$. This design condition is valid for our one aerial robot case of the MAGMaS whose aerial robot is connected at the flexible load tip (i.e., $x = l_f$). This conditions can also be applied to the MAGMaS with multiple aerial robots.

If the aerial robot cannot meet the *control condition*, i.e., $\cos(\theta_{ar}^{\mathcal{L}}) = 0$ or $\theta_{ar}^{\mathcal{L}} = \frac{\pi}{2} + k\pi, k \in \mathcal{Z}$, then the thrust of the aerial robot is aligned to $x$-axis of the load frame $\mathcal{L}$ and subsequently cannot exert force along the deflection direction. This controllability condition impose to control the aerial robot orientation to $\cos(\theta_{ar}^{\mathcal{L}}) \neq 0$. In this paper, to preserve the control condition and to maximize the thrust input along the deflection of the flexible load, we control the aerial robot attitude so that $\bar{\theta}_{ar} = \bar{\theta}_l$, i.e., $\cos\bar{\theta}_{ar}^{\mathcal{L}} = 1$.

The *physical condition* represents identical natural frequency between two different modes. Physically, two vibration modes with identical natural frequency represented as one combined vibration mode. Mathematically, we compute unique vibration mode for each distinct natural frequencies. Therefore, this condition is always satisfied.

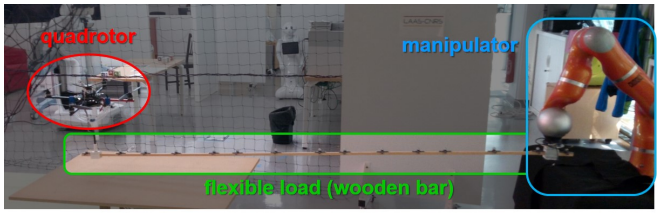


Fig. 4: Ongoing experimental setup for the MAGMaS with a quadrotor, a flexible load and a manipulator.

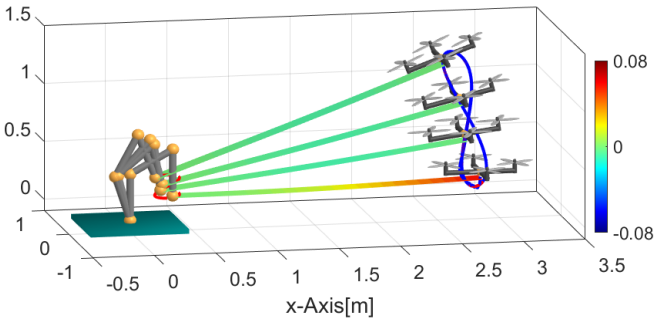


Fig. 5: Snapshot of the eight-shaped trajectory tracking with proposed controller. Color in the flexible load represents its relative deflection w.r.t. a rigid load.

### C. Aerial Robot Control

Vibration suppression can be achieved by the aerial robot control input $\bar{b}_{ar,\delta}\lambda_{ar}$ based on the controllability analysis. We follow two independent control objectives: 1) the aerial robot orientation control for the thrust aligning; 2) the vibration suppression control for the flexible load using the aerial robot thrust. Recall that these two independent controller are available due to the independent rotational dynamics of the aerial robot thanks to the passive rotational joint connector. This rotational joint cannot exert torque between the flexible load and the aerial robot.

First, we design aerial robot orientation controller to align thrust direction with direction perpendicular to the flexible load(i.e., $y$-direction of the flexible load frame $\mathcal{L}$). The control objective is expressed as $\bar{\theta}_{ar} \to \bar{\theta}_l$. This control objective maximize magnitude of the input vector $b_{\delta,ar}$ for the load vibration. For the planar case, the orientation control of the angular rate controlled aerial robot is given as follows

$$\dot{\theta}_{ar} = \dot{\bar{\theta}}_e^d + k(\bar{\theta}_l^d - \bar{\theta}_{ar})$$

where $\bar{\theta}_l^d = \bar{\theta}_e^d + \theta_l$ is the desired load orientation with constant $\theta_l$, $\dot{\bar{\theta}}_l = \dot{\bar{\theta}}_e$ and $k$ is control gain. Note that angular velocity controlled aerial robot can capture many commercially available UAV [3]. For the torque controlled aerial robot, we can exploit a control design proposed in [5].

Next, using the linearized flexible load dynamics and the controllability analysis in Sec. IV, we can design various linear controller to suppress the vibration. Here, we utilize LQR (linear quadratic regulator) to optimally suppress vibration in the MAGMaS,

$$\lambda_{ar} = K_{LQR}\begin{bmatrix}\dot{\tilde{\delta}}\\ \tilde{\delta}\end{bmatrix} + (\Phi K^{-1} b_{\delta,ar})^{-1}\Phi K^{-1} g_\delta \qquad (19)$$

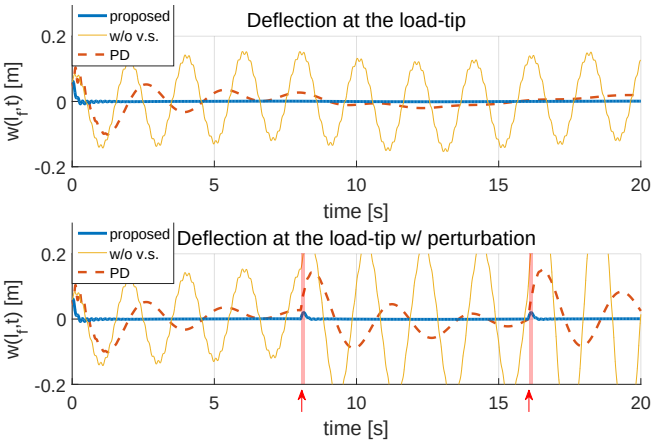


Fig. 6: Simulation results with three different controllers: 1) proposed control; 2) PD control; 3) manipulator control w/o vibration suppression. Trajectory tracking (top) and tracking with perturbation (bottom). An external force is applied to at 8, 16s for the bottom.

where $K_{LQR} \in \Re^{1\times 2m}$ is the control gain based on LQR.

## V. Simulation

To verify the performance of the proposed control scheme, we conduct a set of two simulations. In these simulations, the system parameters are based on real platform data and are as follow: 1) inertia parameters $(m_1, m_2, m_3, m_l, m_{ar}) = (4, 4, 4, 0.591, 1)kg$ and moment of inertia are evaluated as rectangular bar; 2) length $(l_1, l_2, l_3, l_f) = (0.4, 0.4, 0.4, 2.5)m$; 3) bar properties $EI = 51.3Nm^2$, $\rho A = 0.205kg/m$. From this load property, its natural frequencies are given as $(w_{n,1}, w_{n,2}) = (1.44, 8.98)Hz$ which are experimentally retrieved via vibration excitation and FFT analysis. We only consider the first 2-modes as the other higher frequency modes are found negligible by our identification experiments. Here, we utilize two vibration modes $m = 2$ from our preliminary experiments of the wooden load vibration. From the third to higher modes, the magnitude of vibration is negligible and suppressed fast by its own damping.

For the simulation, we assume that the deflection of each modes $\delta_i$ is available. In practice, we can indirectly measure the mode deflection by measuring $w(x,t)$ using MoCap or strain gage for several different points as following

$$\begin{bmatrix}w(x_1,t)\\ w(x_2,t)\end{bmatrix} = \underbrace{\begin{bmatrix}\phi_1(x_1) & \phi_2(x_1)\\ \phi_1(x_2) & \phi_2(x_2)\end{bmatrix}}_{=:\Phi_{12}}\begin{bmatrix}\delta_1(t)\\ \delta_2(t)\end{bmatrix}$$

where $x_i$ are the points which makes non-zero determinant of matrix $\Phi_{12}$.

The first simulation consists in a trajectory tracking task. As mentioned in Sec. IV, we can design the trajectory of the end-effector by considering the flexible load as rigid body. Here, the trajectory is given as $(x_e^d, y_e^d, \bar{\theta}_e) = (0.1\sin(t), 0.1\cos(0.5t), 0.2\sin(0.5t))$. To validate our approach, we compare three different controllers for this trajectory tracking task: 1) proposed controller in (12) and (19); 2) manipulator controller without vibration suppression: $\tau_m$ is same with (12) and $\lambda_{ar}$ is same with (15); 3) PD control

in [18]: $\lambda_{ar}$ is same with (15) and $\tau_m$ satisfies

$$\tau_m = \bar{M}_\xi \ddot{\xi}_d + D_e \dot{e} + K_e e + \bar{g}_e - (J_\xi^{-T} J_f^T(q) - B_{\delta,ar})\tau_{ar}$$

For controller 2 and 3, the aerial robot input is just gravity compensation of the flexible load and the aerial robot. The simulation result are gathered in Fig. 6. Under the tracking controller 2, vibration is not suppressed while control 3 and the proposed controller is suppressing the vibration. Controller 3 can suppress the vibration, however it only relies on energy dissipation, the convergence time is slower than our proposed controller which can directly suppress the vibration using the aerial robot control input $\tau_{ar}$.

The second simulation in Fig. 6 includes perturbations by an external force on the load-tip. The perturbations are given as $(f_x, f_y) = (5, 15)N$ at $t = 8s$ and $t = 16s$ during $0.05s$. In this plot, we exclude the result of controller 2 whose vibration amplitude is too large to compare. Similar to the first simulation, after the perturbation, both controller 3 and our proposed controller can suppress the vibration although the convergence is much slower for controller 3.

Those two simulations validate our proposed approach to leverage MAGMaS's heterogeneous design, by exploiting the aerial robot control input, trajectory tracking performances are increased for flexible load.

## VI. Conclusion

In this paper, we extend results on the MAGMaS, a novel cooperative heterogeneous manipulation system [1], to the case of flexible load manipulation. In particular, we derive the dynamical model of a planar MAGMaS, including vibrations in the long slender load. We then propose a control strategy for both trajectory tracking and effective vibration cancellation by exploiting the dynamical properties of such an under-actuated system for vibration, in particular vibration cancellation is achieved through a linearization scheme. Along the way, the conditions for controllability of the vibrations modes are exhibited. The validity of this approach is demonstrated in two simulations by comparing its performance to the one of previously proposed approaches. The possible next step for this work are the experimental validation for the planar case, the system for which is already in construction, and the extension of the theoretical work to the general 3-dim case with multiple aerial robots.

## References


[1] N. Staub, M. Mohammadi, D. Bicego, D. Prattichizzo, and A. Franchi. Towards robotic MAGMaS: Multiple aerial-ground manipulator systems. In *Proc. IEEE Int'l Conference on Robotics and Automation*, 2017.

[2] R. Mahony, V. Kumar, and P. Corke. Multirotor Aerial Vehicles: Modeling, Estimation, and Control of Quadrotor. *IEEE Robotics & Automation Magazine*, 19(3):20–32, 2012.

[3] C. Ha, Z. Zuo, F. B. Choi, and D. J. Lee. Passivity-based adaptive backstepping control of quadrotor-type uavs. *Robotics and Automation Systems*, 62(9):1305–1315, 2014.

[4] A. Franchi, C. Secchi, M. Ryll, H. H. Bülthoff, and P. Robuffo Giordano. Shared control: Balancing autonomy and human assistance with a group of quadrotor UAVs. *IEEE Robotics & Automation Magazine*, 19(3):57–68, 2012.

[5] D. J. Lee, A. Franchi, H. I. Son, C. Ha, H. H. Bulthoff, and P. R. Giordano. Semiautonomous haptic teleoperation control architecture of multiple unmanned aerial vehicles. *IEEE Transactions on Mechatronics*, 18(4):1334–1345, 2014.

[6] DJI. `www.dji.com/`, Accessed: 2018-03-02.

[7] Intel Shooting Star. `https://www.intel.com/content/www/us/en/technology-innovation/aerial-technology-light-show.html`, Accessed: 2018-03-02.

[8] H.-N. Nguyen, S. Par, J. Park, and D. J. Lee. A novel robotic platform for aerial manipulation using quadrotors as rotating thrust generators. *IEEE Transactions on Robotics*, 2018 (to apear).

[9] K. Kondak, F. Hubert, M. Schwarzbach, M. Laiacker, D. Sommer, M. Bejar, and A. Ollero. Aerial manipulation robot composed of an autonomous helicopter and a 7 degrees of freedom industrial manipulator. In *Proc. IEEE Int'l Conference on Robotics and Automation*, pages 2108–2112, 2014.

[10] C. Korpela, M. Orsag, M. Pekala, and P. Oh. Dynamic stability of a mobile manipulating unmanned aerial vehicle. In *Proc. IEEE Int'l Conference on Robotics and Automation*, pages 4922–4927, 2012.

[11] M. Tognon, B. Yuksel, G. Buondonno, and A. Franchi. Dynamic decentralized control for protocentric aerial manipulators. In *Proc. IEEE Int'l Conference on Robotics and Automation*, pages 6375–6380, 2017.

[12] G. Darivianakis, Kostas Alexis, Michael Burri, and R. Siegwart. Hybrid predictive control for aerial robotic physical interaction towards inspection operation. In *Proc. IEEE Int'l Conference on Robotics and Automation*, pages 53–58, 2014.

[13] Q. Lindsey, D. Mellinger, and V. Kumar. Construction of cubic structures with quadrotor teams. In *Robotics: Science and Systems*, 2011.

[14] Koushil Sreenath, Nathan Michael, and Vijay Kumar. Trajectory generation and control of a quadrotor with a cable-suspended load-A differentially-flat hybrid system. In *Proc. IEEE Int'l Conference on Robotics and Automation*, pages 4888–4895, 2013.

[15] H. Yang and D. J. Lee. Hierarchical Cooperative Control Framework of Multiple Quadrotor-Manipulator Systems. In *Proc. IEEE Int'l Conference on Robotics and Automation*, pages 4656–4662, 2015.

[16] M. Mohammadi, A. Franchi, D. Barcelli, and D. Prattichizzo. Cooperative aerial tele-manipulation with haptic feedback. In *Proc. IEEE/RSJ Int'l Conference on Intelligent Robots and Systems*, pages 5092–5098, 2016.

[17] B. Siciliano and W. J. Book. A singular perturbation approach to control of lightweight flexible manipulators. *The International Journal of Robotics Research*, 7(2):79–90, 1988.

[18] A. D. Luca and B. Siciliano. Regulation of flexible arms under gravity. *IEEE Transactions on Robotics and Automation*, 9(4):463–467, 1993.

[19] D. J. Inman. *Engineering Vibration*. Pearson, 2008.

[20] A. D. Luca and B. Siciliano. Closed-form dynamic model of planar multilink lightweight robots. *IEEE Transactions on Systems, Man, and Cybernetics*, 21(4):826–839, 1991.

[21] J. Cheong, W. K. Chung, and Y. Youm. Inverse kinematics of multilink flexible robots for high-speed applications. *IEEE Transactions on Robotics and Automation*, 20(2):269–282, 2004.

[22] Y. Nakamura, H. Hanafusa, and T. Yoshikawa. Task-priority based redundancy control of robot manipulators. *The International Journal of Robotics Research*, 6(2):3–15, 1987.